Supplementary Material for

EPFR-Mediated Enhancement of Atmospheric Oxidants Dominates the Photochemical Transformation of Acenaphthylene on Mineral Dusts

Ying Hua [a], Ting Xue [a], Kanglu Li *[,b], Qin Ren [a], Shiyong Mou [a], Lvcun Chen [b], Fan Dong*[,a]

[a] Research Center for Carbon-Neutral Environmental & Energy Technology, Institute of Fundamental and Frontier Sciences, University of Electronic Science and Technology of China, Chengdu 611731, China.

[b] School of Environmental Science and Engineering, Southwest Jiaotong University, Chengdu 611756, China.

* Corresponding author: Fan Dong (dongfan@uestc.edu.cn), Kanglu Li (kangluli@swjtu.edu.cn).

This file includes:

Supplementary Text

Figures S1 to S6

Tables S1 to S3

References (1 to 6)

Table of Content

Supplementary Texts

Text S1. HPLC Analysis

The residual ACY after 3 h of photoreaction was extracted from the glass slide with 2 mL of methanol and quantified by HPLC (LC-20 HPLC, Shimadzu) with a C18 column. The detection wavelength of the UV detector was set at 280 nm. The mobile phases were 50% deionized water and 50% acetonitrile at a flow rate of 1.5 ml min^{-1}. The conversion of ACY was determined by

$$1-\frac{C_t}{C_0}=1-\frac{A_t}{A_0} \quad (1)$$

Where C_t and C_0 denote the ACY concentration at time t and time 0, respectively, and A denotes the peak area at the corresponding time.

The benzoic acid oxidation reaction can be quantitatively used to determine ·OH production, where the total ·OH yield is calculated based on the accumulated amount of the oxidation product p-hydroxybenzoic acid (*p*-HBA), using a conversion factor of 5.87 for the calculation. The HPLC mobile phase consisted of acetonitrile/H_3PO_4 (4:6, v/v) with a flow rate of 1 mL min^{-1}, and the detection wavelength was set at 256 nm (Ma et al., 2025).

Text S2. Quenching Experiments of Active Species

Potassium iodide (KI), potassium dichromate ($K_2Cr_2O_7$), tertiary butyl alcohol (TBA), 1,4-p-benzoquinone (PBQ), and L-tryptophan were used to quench holes (h^+), electrons (e^-), ·OH, $\cdot O_2^-$, and $^1O_2$, respectively. Specifically, a mixture of ACY (0.1 g), mineral particles (0.2 g), and quencher was uniformly coated on the surface of the glass slide. Then, the mixed samples were tested in the photochemical reaction to determine the active species driving the conversion of ACY.

Text S3. *In Situ* DRIFTS Measurements

In situ DRIFTS measurement was performed using INVENIO-R fourier transform infrared spectrometer (Bruker) equipped with *in situ* diffuse reflectance cell (Harrick) and a high-temperature reaction chamber (HVC). The sample was placed in the chamber and pre-treated with argon gas at 55°C for 30 min to remove surface impurities. Zero air was then introduced as the carrier gas. A Xenon lamp with a wavelength range of 300-800 nm (300 W, Bobei BBZM-1) was used for irradiation. IR spectra were recorded as a function of time to investigate the photochemical transformation of ACY.

Text S4. DFT Calculations

DFT calculations were performed using the Vienna ab initio simulation package (VASP 6.2.1). The electron exchange and correlation interactions are described by the Perdew-Burke-Ernzerhof generalized gradient approximation (PBE-GGA). To avoid the interaction between slabs during ACY adsorption, models with a large surface were constructed (Figure S1). Considering the large size of the model, a K-point mesh of (1 × 1 × 1) was adopted throughout the structure optimization. All atoms were converged to 0.03 eV $Å^{-1}$ and 1×10^{-4} eV. Van der Waals effect was corrected by the D3 method (Grimme et al., 2010). Hubbard (U) correction was applied to correct the strong electronic correlation of the Fe/Ti 3*d*-electrons, using U = 4 eV for Fe and 3.5 eV for Ti (Arroyo-de Dompablo et al., 2011; Cococcioni and De Gironcoli, 2005; Guo and Barnard, 2011).

Text S5. UV-vis DRS

The concentration of H_2O_2 generated by the ACY/TiO_2 system after 1 h of illumination was determined using a PTO solution ($C_4K_2O_9Ti\cdot2H_2O$) and UV-Vis DRS (UV-2450, Shimadzu). The maximum response wavelength was observed at 400 nm, and the H_2O_2 concentration was calculated based on the absorbance measured at this wavelength (Lee et al., 2019).

Text S6. Steady-state photoluminescence (PL) spectra

Steady-state photoluminescence (PL) spectra were measured with a Hitachi F-7000 spectrometer (Shimadzu). The excitation wavelength used is 365 nm, with a spectral range of 400-500 nm.

Supplementary Figures

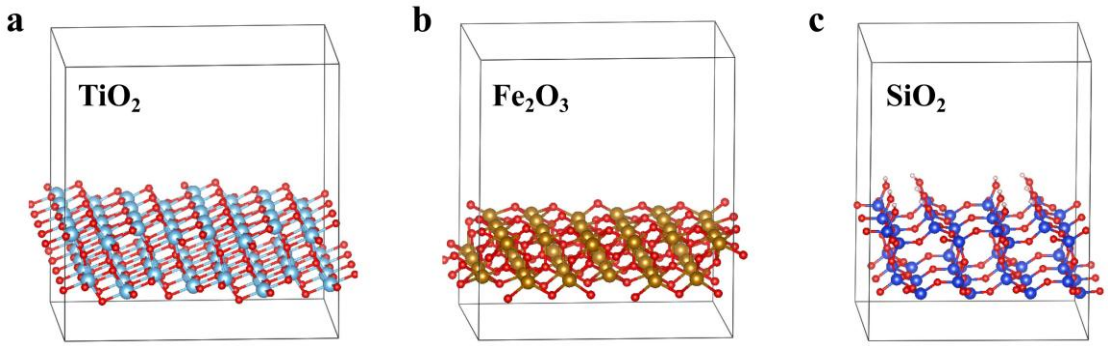

Fig. S1. Optimized models of (a) TiO_2, (b) Fe_2O_3, and (c) SiO_2 for DFT calculations.

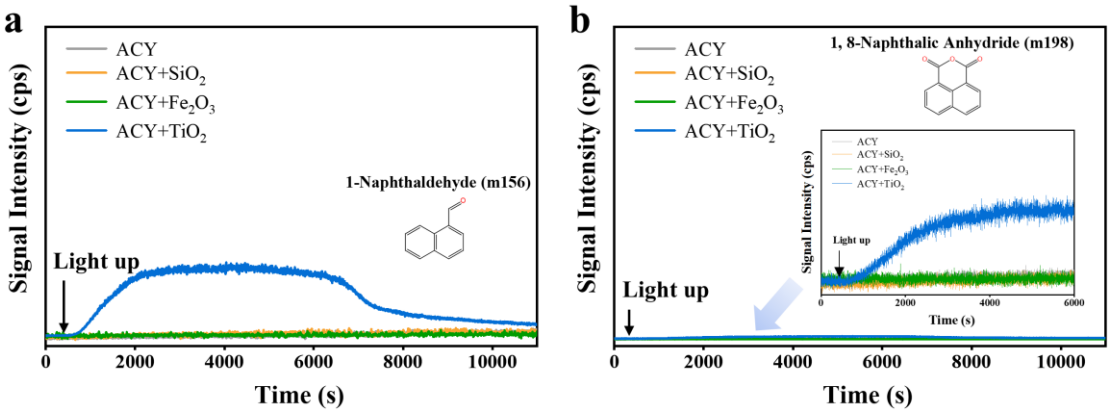

Fig. S2. PTR-TOF-MS spectra of gaseous intermediates in the outlet gas stream of the ACY/particle systems.

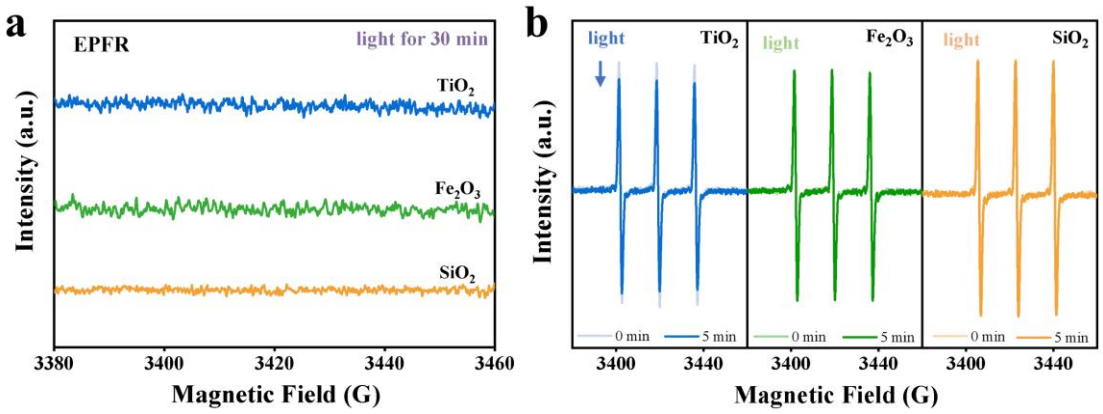

Fig. S3. Comparison of (a) EPFR and (b) TEMPO spin-trapping EPR spectra of mineral dusts.

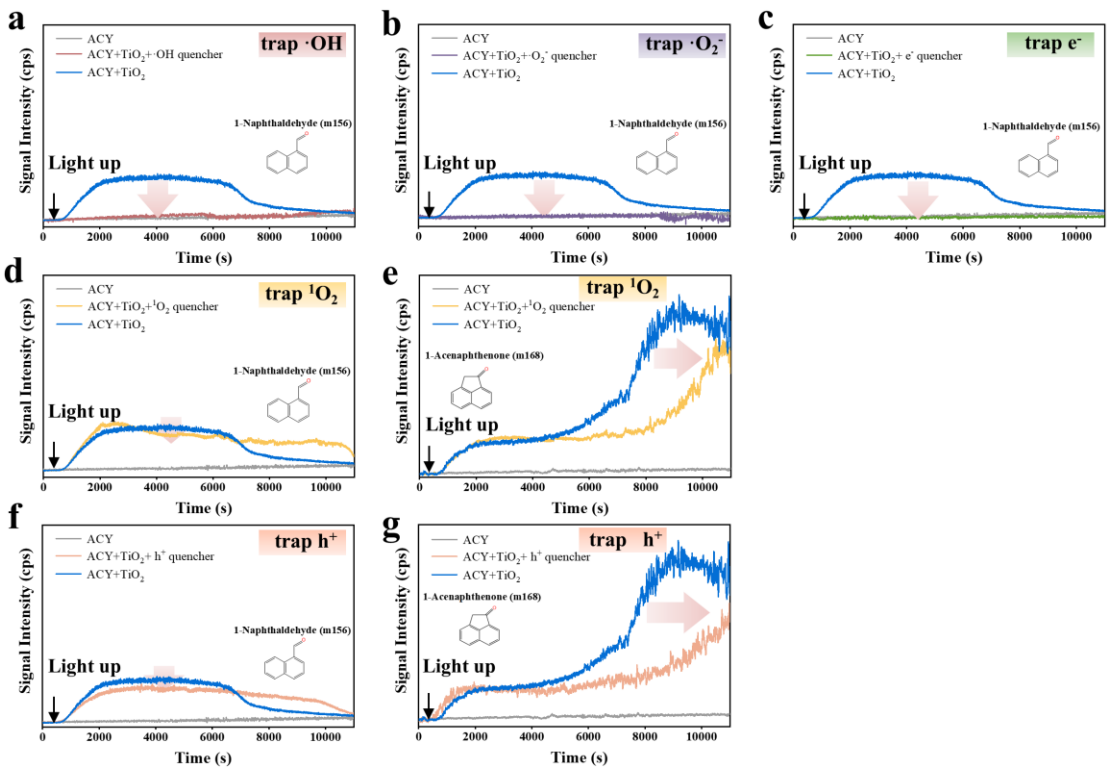

Fig. S4. PTR-TOF-MS spectra of the photochemical products in quenching experiments: (a) TBA-·OH, (b) PBQ-·O_2^-, (c) $K_2Cr_2O_7$-e^-, (d, e) L-tryptophan-$^1O_2$ and (f, g) KI-h^+.

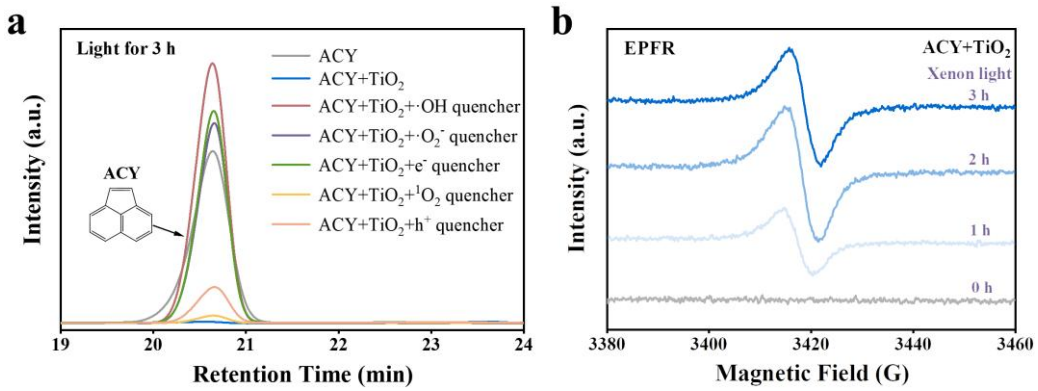

Fig. S5. (a) Change in ACY concentration after quenching active species, detected by HPLC. (b) Changes in EPFR signal formed by ACY/TiO_2 system under prolonged light irradiation.

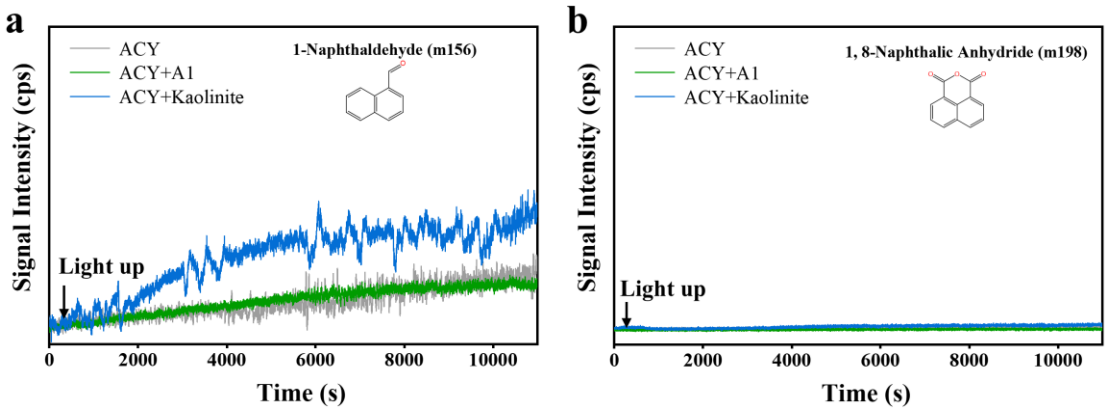

Fig. S6. PTR-TOF-MS spectra of photochemical products during the transformations of ACY on the surfaces of A1 dust and kaolinite dust.

Supplementary Tables

Table S1. ·OH concentration generated by the ACY/TiO_2 system

·OH Concentration (10^{-3} μM)			
ACY	TiO_2	ACY+TiO_2	·OH contributed by the EPFR pathway
0.04	0.76	2.63	1.83
0.04	1.57	6.2	4.59
0.08	0.04	6.2	6.08

Table S2. Chemical composition and weight ratio of natural Kaolinite.

Natural Kaolinite	
Chemical Composition	Percentage by weight
SiO_2	56.93
Al_2O_3	37.49
Fe_2O_3	1.81
CaO	0.01
K_2O	0.06
FeO	0.15
MgO	0.03
TiO_2	**3.43**
P_2O_5	0.05

Table S3. Chemical composition and weight ratio of A1 dust.

A1 dust	
Chemical Composition	Percentage by weight
SiO_2	69.0 ~ 77.0
Al_2O_3	8.0 ~ 14.0
Fe_2O_3	**4.0 ~ 7.0**
CaO	2.5 ~ 5.5
K_2O	2.0 ~ 5.0
Na_2O	1.0 ~ 4.0
MgO	1.0 ~ 2.0
TiO_2	0.5 ~ 1.0
P_2O_5	0

Reference

Arroyo-de Dompablo M E, Morales-García A, Taravillo M (2011). DFT + *U* calculations of crystal lattice, electronic structure, and phase stability under pressure of TiO_2 polymorphs. The Journal of Chemical Physics, 135: 054503

Cococcioni M, De Gironcoli S (2005). Linear response approach to the calculation of the effective interaction parameters in the LDA + U method. Physical Review B, 71: 035105

Grimme S, Antony J, Ehrlich S, Krieg H (2010). A consistent and accurate *ab initio* parametrization of density functional dispersion correction (DFT-D) for the 94 elements H-Pu. The Journal of Chemical Physics, 132: 154104

Guo H, Barnard A S (2011). Modeling the iron oxides and oxyhydroxides for the prediction of environmentally sensitive phase transformations. Physical Review B, 83: 094112

Lee J K, Walker K L, Han H S, Kang J, Prinz F B, Waymouth R M, Nam H G, Zare R N (2019). Spontaneous generation of hydrogen peroxide from aqueous microdroplets. Proceedings of the National Academy of Sciences, 116: 19294-19298.

Ma H, Chen Y, Wang Y, Feng C, Dang Z, Zhu S, Sun K (2025). Synergistic Photochemistry of Dissolved Black Carbon Mediated by Iron: A Critical Pathway for Enhancing Hydroxyl Radical Generation. Environ. Sci. Technol. 59, 24430-24440.